

Observation of laser-induced microscale knotted and unknotted vortex filaments on vaporizing tantalum surface

S. Lugomer

Ruder Bošković Institute, Bijenička c. 54, 10001 Zagreb, Croatia

(Received 15 December 1995; revised manuscript received 29 April 1996)

Laser-induced Ta-surface superheating on a ns time scale is connected with the formation of a spinodal fluid which decomposes into a gaseous phase through microexplosions, generating vortex filament structures on the vaporizing surface. Vortex filaments associated with the Reynolds number $Re \sim 10^3 - 10^4$ are organized into regular, quasiregular, or chaotic structures. Homotopic operations transfer these structures into irreducible ones of a simple closed-loop type, showing that all of them are embedded in a three-dimensional torus either as a vortex ring (unknotted knot), as a cloverleaf (trefoil knotted knot), or as Hopf links (knotted knot). [S0163-1829(96)08432-9]

The paper deals with experimental evidence of generation and organization of vortex filaments in the explosive decomposition of a spinodal fluid (liquid Ta) into a gaseous phase on the time scale ≤ 10 ns. Spinodal fluid^{1,2} is generated during surface superheating of metals in high-power, short-time-scale laser-metal interactions when the surface layer behaves as a dielectric.³ It thus, becomes transparent enabling a deep volume absorption of a laser beam.³ The vapor pressure above the surface prevents boiling, and causes superheating of the liquid metal.^{1,3}

The calculations of Grosse⁴ (based on the van der Waals theory) have shown that superheating may in principle occur for all metals, but that the spinodal curve for some of them is flat rather than cusplike. However, for refractory metals (Ti, Ta, Mo, etc.) the cusp is large, and superheating may reach even $10^3 - 10^4$ K. The system is pushed into a metastable region of a thermodynamic diagram, where thermal conductivity $k \rightarrow 0$, and specific heat $Cp \rightarrow \infty$.^{1,2} Since fluctuations play a crucial role in the metastable phase, the system is not stable, and exists only for a short time, after which it decomposes into a gaseous phase through microexplosions of surface bubbles, characteristic of the onset of "volume" boiling. As usually assumed, this transition occurs at $Q \approx 10^8$ W/cm².

The transition from planar to "volume" boiling is not a well-elucidated problem from the aspect of the phase diagram, nor from the aspect of surface dynamics and the corresponding surface morphology. Ultrafast cooling after pulse termination causes the surface morphology to stay permanently frozen, thus enabling *a posteriori* analysis.

Recent studies of these problems on metals,⁵ semiconductors,⁶ and superconductor ceramics^{7,8} shed more light on superheating on a ns time scale. In spite of the difference in the absorption process and the superheating (surface or subsurface) in these materials, the surface morphology associated with fully developed volume boiling is the same. The most intriguing aspect relates to the onset of volume boiling (not fully developed) associated with the reach spectrum of dynamic phenomena, and generation of a strange morphology.⁵

Our studies with a Q-switched Nd:YAG (yttrium aluminum garnet) laser, with 10 ns at half width at half-maximum,

at a spot size $\sim 3-4$ mm, $Q \approx 10^7$ W/cm² performed on small samples $\sim 1 \times 1 \times 0,05$ cm of Ta, indicate that small regions of volume boiling may appear inside the planar boiling, i.e., at the laser power density $Q < Q_{\text{volume boiling}}$. For large samples, however, volume boiling seems to be absent under the same experimental conditions. In addition, the contour of the volume boiling regions on the small samples strongly depends on the location of the laser spot; that is, it is different in the center, in the corner, or near the sidewall of the sample. This strongly indicates the role of shock waves in the generation of regions of the spinodal fluid, and therefore of regions of volume boiling inside the planar one.⁹ In large samples, the stress waves suffer a gradual decay, and being reflected from the sample sidewalls, they return back into the laser-interaction space with delay, after the pulse termination. In small samples, however, the attenuation is insignificant, and reverberated waves return into the interaction space before the pulse termination, with almost the same energy. This gives rise to regions of very high pressure, and with the spinodal characteristics of liquid metal. Thus regions of volume boiling coincide with regions of high pressure, established by superposition of the shock waves.⁹

The explosion of bubbles on the vaporizing surface of tantalum generates vortex filaments organized into spatial structures, ranging from circular (vortex rings) to very complex, and even to chaotic ones. The vortex ring as the most simple structure exhibits a rotation of each vertical element around the curved axis of the figure. The flow of the subsurface fluid separates at the edge of the explosion crater; a cylindrical vortex sheet forms, and rolls up into a vortex ring. The fluid velocity associated with microexplosions is comparable with the velocity of the expelled vapor in laser-driven vaporization, $v \sim 10^5 - 10^6$ cm/s,¹ which gives high Reynolds numbers $Re \sim 10^3 - 10^4$. Similar Reynolds numbers were obtained in experiments under highly controlled conditions (Reed¹⁰ and Widnall and Sullivan¹¹).

Typical examples of the spatial structures developed in the bubbling zones, for the laser spot, are shown in Figs. 1(a) and 1(b). The spatial structure consists of a number of vortex rings which densely [Fig. 1(a)] or not densely [Fig. 1(b)] cover the surface, and resemble a sheet of small-scale structures of vorticity in a turbulent field.

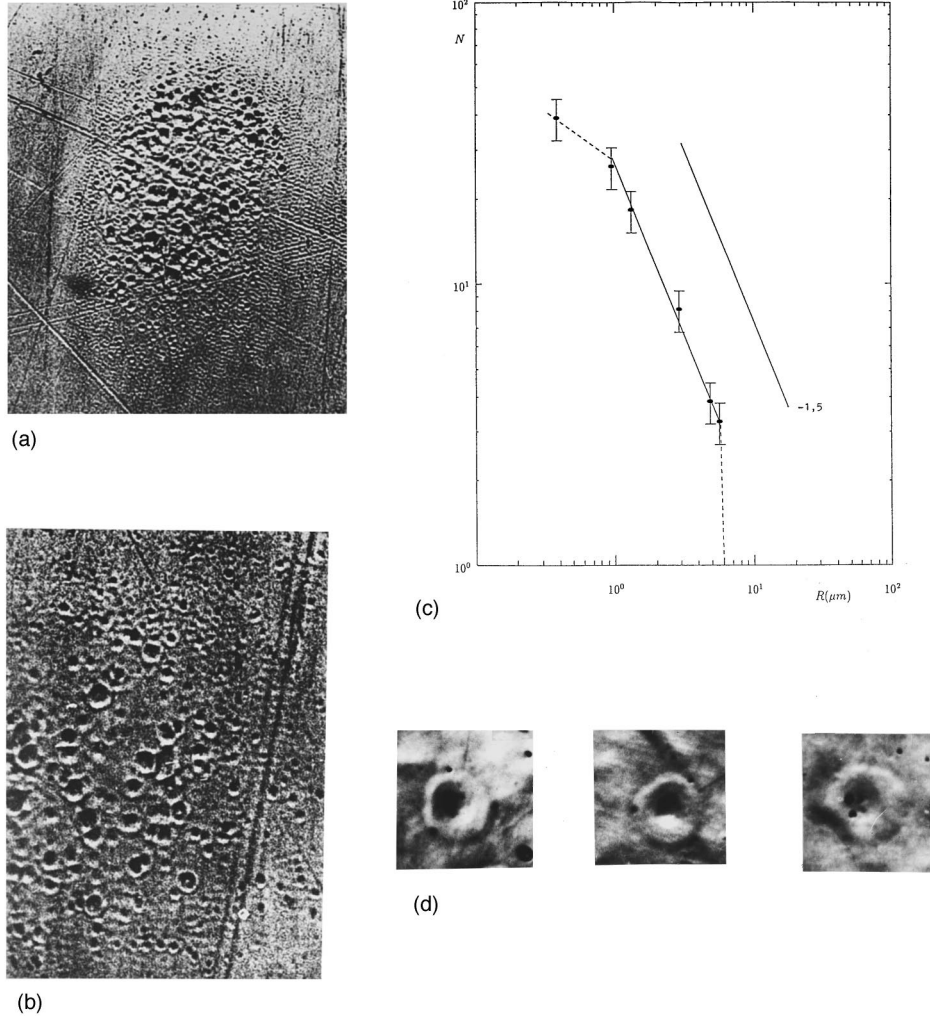


FIG. 1. Local bubbling zone on the Ta surface. Generation of vortex rings of different radii. (a) One of small bubbling zones. $M \sim 500x$. (b) A part of another bubbling zone. $M \sim 1100x$. (c) Distribution of radii for the vortex rings. (d) Vortex ring on a boiling Ta surface. The vortex core becomes gradually more and more flat. (i) The side oscillations which represent the azimuthal instability appear on the circumference of the vortex ring. (ii) The instability involves the appearance and amplification of azimuthal waves around the circumference of the ring. (iii) The waves may subsequently break down to turbulence if their amplitude is large enough. Growth of azimuthal instability is clearly seen, but a transition to turbulence does not take place.

The distribution of the vortex radii R was found to follow the scaling relation

$$N(R) = R^{-\alpha}, \quad (1)$$

with $\alpha \sim 1.5$, which holds for all ring vortices, except for the smallest and largest ones [Fig. 1(c)].

A more precise determination of α requires a larger magnification. However, a larger magnification causes the edges of the vortex rings to become hazy, and the error bar increases.

The vortex ring is unstable. The instability sets in on the perimeter leading to a transformation of a laminar vortex ring into a turbulent one. The transformation occurs through an azimuthal instability seen as a sinusoidal oscillation on the circumference of the vortex ring. This process is accompanied by a ring flattening that occurs through elliptical deformation of the vortex filament. [Fig. 1(d)]. The sinusoidal perturbation amplifies with the factor α , given by¹¹

$$\alpha = \frac{\Gamma}{4\pi R^2} n \sqrt{1-n^3} \ln(\eta R), \quad (2)$$

where Γ is the total vorticity, n the number of maxima of disturbance of the vortex ring, η the vortex filament diameter, and R the radius of the ring. Although it is difficult to determine n for very small rings, we estimated it to be 3 or 5 for a majority of vortex rings. This should be compared with the vortex rings obtained on a much larger spatial scale by Glezer,¹² Reed,¹⁰ and Fohl and Turner.¹³

In the present experiment the azimuthal instability does not reach the stage which causes a transition of the vortex ring into a fully turbulent state. Development of a fully turbulent state would probably require a time scale larger than the pulse duration (10 ns). Instead, deformation of the vortex filament becomes very intensive. As a consequence rings become flat, and are embedded into the background fluid. The vortex core flattening is caused by viscosity effects which start to increase after the laser pulse reaches a maximum.

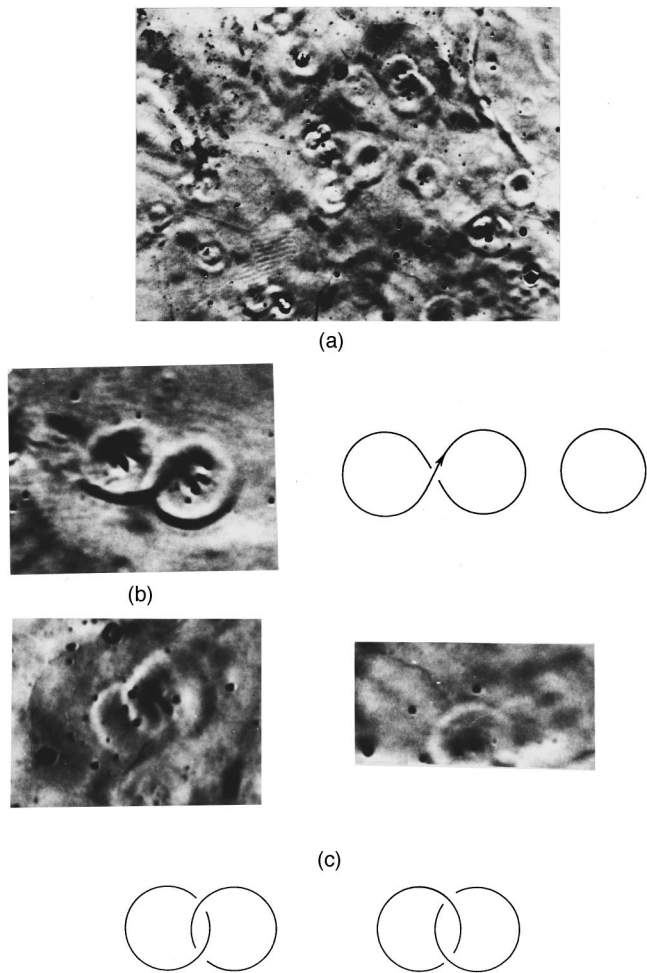


FIG. 2. (a) Local bubbling zone showing different types of the vortex filament organization than Fig. 1. $M \sim 1100x$. (b) The “eight-type organization. $M \sim 2300x$. (i) Symbolic representation of the filament by a curve. (ii) Folding of the loop transforms the structure into a simple vortex ring. (c) The crossed ring organization of the vortex filaments. (Overcrossing and undercrossing). (i) Symbolic representation of filaments indicates the knotted vortices of the Hopf-link type.

Also, the surface tension starts to increase abruptly because of ultrafast surface cooling at the end of the laser pulse.

A different pattern of spatial structures, which (in addition to the vortex rings) contains a vortex filament organization of various complexity levels, can be seen in Fig. 2(a). Some of the structures, showing a complex but still regular organization of vortex filaments of the closed-loop type, are shown in Figs. 2(b) and 2(c). Both cases represent the vortex rings embedded into a three-dimensional (3D) torus: the first one is unknotted, and the second one knotted.^{14–17}

Additional types of complex organizations of vortex filaments are shown in Figs. 3 and 4. These structures are the result of motion of the vortex segments in different planes with different velocity. The amplitude of the disturbance that causes the motion of vortex core segments is much larger than that of the core radius, and it is associated with local shear flow. This is the result of strong shocks imposed by the laser pulse on the fluid. The shock waves which interact with vortex filaments are generated in the center of the beam, but they can be also reflected, refracted, or dispersed from the

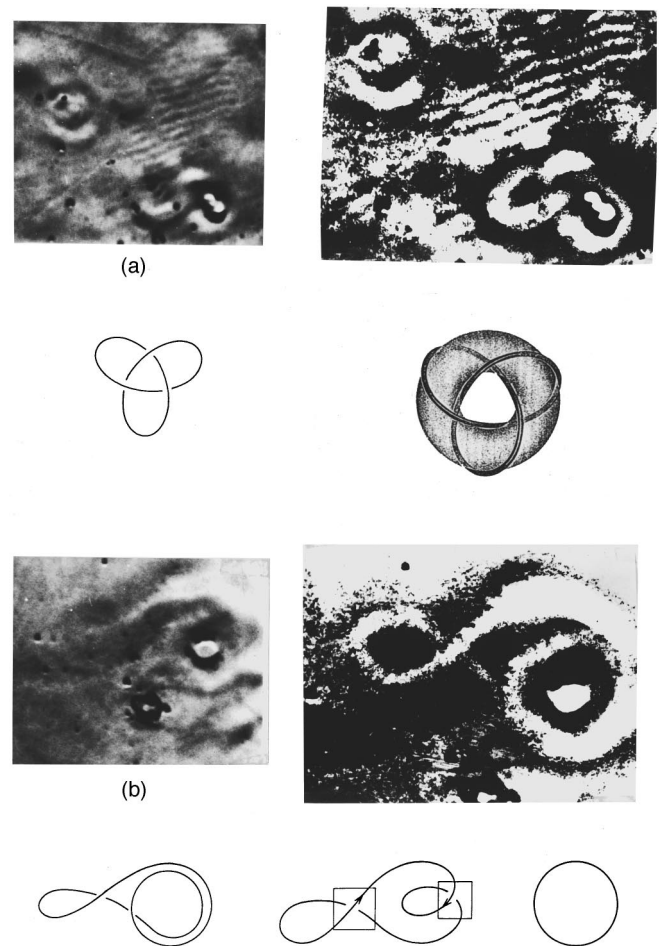


FIG. 3. Complex organization of the vortex filament. (a) Micrograph of the knotted vortex ring (low right corner). $M \sim 2300x$. (i) Magnified micrograph after numerical filtration by the image analyzer. The knotted vortex is identified as the asymmetrical cloverleaf with one loop shrunk. (ii) Symbolic representation of the cloverleaf-knotted vortex filament. (iii) Schematic illustration of embedding of the knotted filament into a 3D toroidal space. (b) Another type of complex organization of vortex filament. $M \sim 2300x$. (i) Magnified micrograph after numerical filtration. (ii) Symbolic representation of the vortex filament by a curve. (iii) Folding the large loop to the right and the small one to the left reveals a more simple homotopic structure. (iv) The final stretching operation transforms the structure into a simple vortex ring (the unknotted knot).

sample walls, grain boundaries, or defects in the underlying solid. These shock waves cause deformation, stretching, squeezing, winding, and folding of the vortex filament segments, thus giving rise to a chaotic spatial organization.

Systematization of the vortex filament organization is based on knot theory,^{14,15} and the assumption that each particular knot has a complexity level, or skewness level, which is given by the number of topological operations needed to reconstruct the basic homotopic structure. According to this principle, the vortex filament organization shown in Figs. 2–4 follows an increasing level of topological complexity.¹⁵

Homotopic operations reveal that every chaotic structure may be transferred into a basic structure of a simple closed-loop type. They are embedded in a 3D torus, and appear to

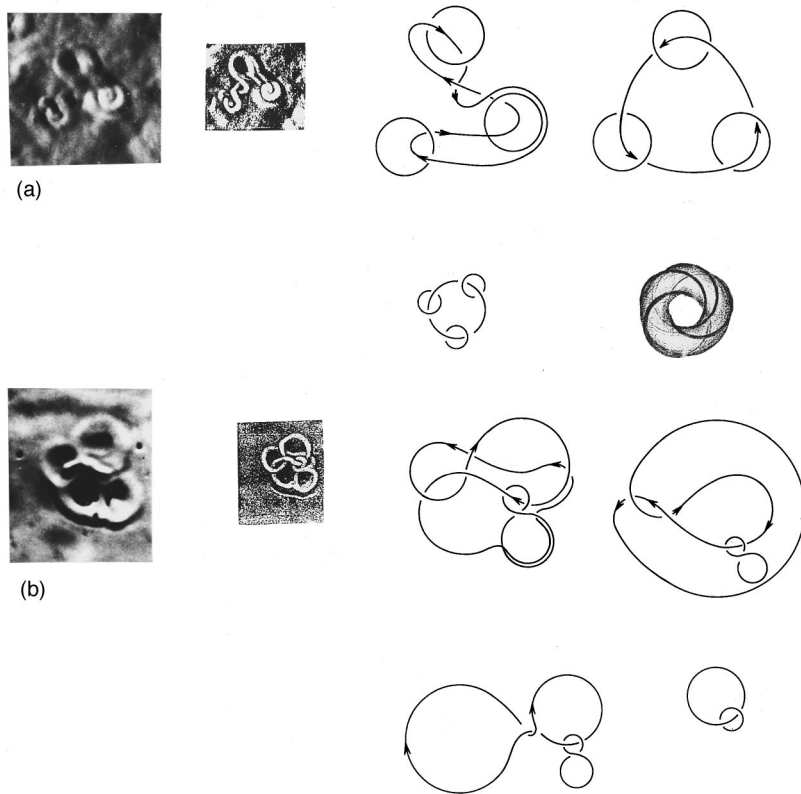


FIG. 4. Chaotic organization of the vortex filament. (a) Micrograph of chaotic filament organization. $M \sim 1100x$. (i) Micrograph after numerical filtration. (ii) Symbolic representation of the vortex filament by a curve. (iii) By folding and stretching the left and right loops, the structure is transformed into a simple one, indicating the three Hopf links. (iv) Symbolic representation of three Hopf links (knotted knots). (b) Another type of chaotic vortex filament organization. (i) Micrograph after numerical filtration. (ii) Symbolic representation of the filament by a curve. (iii) By stretching the large undercrossing loop to the right, the structure becomes more simple. (iv) By folding the large loop to the left, the structure is further simplified. (v) In the final homotopic operation the structure appears to be the Hopf link, i.e., the knotted knot also embedded in 3D toroidal space.

be a vortex ring (unknotted knot), a cloverleaf (trefoil knotted knot), or Hopf links (knotted knot).

The background field contours have too small an intensity to be reliably analyzed. Magnetification and contrasting of the flowlines give patterns similar to those obtained in numerical simulations by Ruetsch and Maxey.¹⁸ Most of the flow lines of the background field are merged in the moment when the laser pulse is switched off. This means that their dissipative time scale is very short, i.e., shorter than the pulse

duration. Therefore, the turbulent field of the vaporizing tantalum surface, generated by the short high-power laser pulse, may be characterized by two time scales: The first one is for the background turbulent field with fast turbulent cascades which ends a stratified fluid. The second one is the long-time scale (comparable to the pulse duration) of the knotted and unknotted vortex filaments, associated with microexplosions of spinodal fluid.

¹A. A. Samokhin, in *Absorption of Laser Radiation in Condensed Matter*, Trudi Iofan, Academy of Sciences USSR, edited by V. B. Fedorov (Publisher, Moscow, 1988) (in Russian).

²A. A. Samokhin and A. B. Uspensky, *Zh. Éksp. Teor. Fiz.* **73**, 1025 (1977).

³Y. V. Afanasiev and O. N. Krokhn, *Zh. Éksp. Teor. Fiz.* **52**, 966 (1967).

⁴A. V. Grosse, *J. Inorg. Chem.* **22**, 23 (1961).

⁵S. Lugomer and A. Maksimović, *Philos. Mag.* (to be published).

⁶R. K. Singh and J. Narayan, *Phys. Rev. B* **41**, 8843 (1990).

⁷D. Bhattacharya, R. K. Singh, and P. H. Holloway, *J. Appl. Phys.* **70**, 5433 (1991).

⁸R. K. Singh, O. W. Holland, and J. Narayan, *J. Appl. Phys.* **68**, 233 (1990).

⁹S. Lugomer (unpublished).

¹⁰H. L. Reed, *Phys. Fluids* **31**, 2383 (1988).

¹¹S. Widnall and J. P. Sullivan, *Proc. R. Soc. London Ser. A* **332**, 335 (1973).

¹²A. Glezer, *Phys. Fluids* **31**, 3532 (1988).

¹³T. Fohl and J. S. Turner, **18**, 433 (1975).

¹⁴L. Neuwirth, *Sci. Am.* **84** (1979).

¹⁵V. F. R. Jones, *Sci. Am.* **52** (1990).

¹⁶M. W. Hirsch, *Differential Topology* (Springer-Verlag, New York, 1976).

¹⁷A. H. Wallas, *Differential Topology* (Benjamin, New York, 1968).

¹⁸G. R. Rutesh and M. R. Maxey, *Phys. Fluids A* **4**, 2747 (1992).